

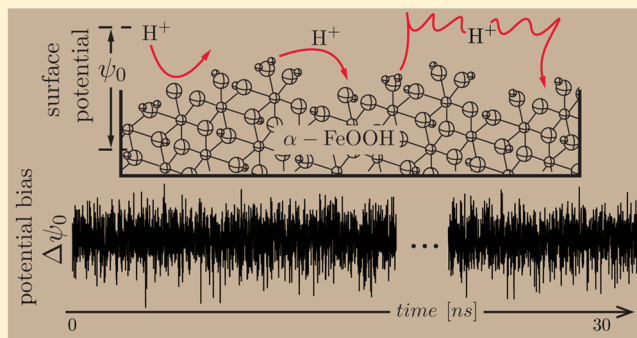
Proton Dynamics on Goethite Nanoparticles and Coupling to Electron Transport

Piotr Zarzycki,*[†] Dayle M. Smith,[‡] and Kevin M. Rosso[‡]

[†]Institute of Physical Chemistry, Polish Academy of Sciences, 01-224 Warsaw, Poland

[‡]Pacific Northwest National Laboratory, Richland, Washington 99354, United States

ABSTRACT: The surface chemistry of metal oxide particles is governed by the charge that develops at the interface with aqueous solution. Mineral transformation, biogeochemical reactions, remediation, and sorption dynamics are profoundly affected in response. Here we report implementation of replica-exchange constant-pH molecular dynamics simulations that use classical molecular dynamics for exploring configurational space and Metropolis Monte Carlo walking through protonation space with a simulated annealing escape route from metastable configurations. By examining the archetypal metal oxide, goethite (α -FeOOH), we find that electrostatic potential gradients spontaneously arise between intersecting low-index crystal faces and across explicitly treated oxide nanoparticles at a magnitude exceeding the Johnson–Nyquist voltage fluctuation. Fluctuations in adsorbed proton density continuously repolarize the surface potential bias between edge-sharing crystal faces, at a rate slower than the reported electron–polaron hopping rate in goethite interiors. This suggests that these spontaneous surface potential fluctuations will control the net movement of charge carriers in the lattice.



1. INTRODUCTION

Charged Hydrated Metal Oxide Surfaces. Metal oxides immersed in water develop a surface charge due to proton uptake by surface oxygen atoms and by dissociative water sorption.¹ Surface protonation and all resulting electrostatic interfacial properties are controlled by the pH, including ion adsorption/desorption and dissolution/growth.^{1,2}

Metal oxide surface charge is typically treated with models that describe average protonation behavior at thermodynamic equilibrium, such as surface complexation models (SCMs). SCMs consist of assumed surface site types and proton affinities, surface–ion binding reactions, and the structure of the electrical double layer (i.e., specific charge distribution at the interface).^{1,3–5}

However, to understand interfacial chemistry at the atomic scale, such models are inadequate, because actual interfacial structure and chemical dynamics are neglected. The primarily incentive for the presented work is the question whether surface protonation/deprotonation reactions can influence interfacial electron-transfer (ET) energetics and rates. It has been shown by isotopic labeling that at neutral pH aqueous Fe(II) ions and crystallites of the Fe(III)-oxyhydroxide, goethite (α -FeOOH), exchange iron atoms completely within 30 days.^{6–10} Goethite is evidently fully recrystallized during interaction with Fe(II); however, its physical properties and characteristics of particle ensembles appear unchanged.^{10,11} It was thus proposed, as was deduced for Fe(II) interaction with hematite (α -Fe₂O₃) crystals,¹² that this occurs by a mechanism of adsorption and

oxidation of Fe(II) from solution by the goethite solid, yielding Fe(III) atom addition, connected to reductive release of goethite Fe(III) as aqueous Fe(II) by conduction of injected electrons through the goethite lattice. Even though iron oxides are poor conductors with very large resistivity (e.g., $2 \times 10^6 \Omega$ for hematite¹³ and $16 \times 10^6 \Omega$ for goethite¹³), they are capable of conducting electrons in the form of small polarons.^{14,15} Electron–small polaron hopping rates in goethite were recently predicted from first-principles modeling to be approximately 10^9 s^{-1} ,¹⁶ whereas in hematite they range between 10^8 and 10^{12} s^{-1} depending on crystallographic direction.^{17,18}

Aspects of this phenomenon are problematic from the standpoint of SCMs. First, it has been recently shown^{19,20} that at pH decreasing below the point of zero charge (PZC), Fe atom exchange still occurs, even though the extent of Fe isotopic mixing declines and Fe(II) sorption is energetically unfavorable. This suggests that, despite average electrostatically excluded net Fe(II) adsorption at equilibrium, a fraction of Fe(II) can still adsorb and transfer electrons into goethite. Second, a driving force for the ET reactions and electron conduction through goethite crystallites is not thermodynamically defined in the absence of a surface potential bias; it can be argued that no persistent surface potential bias exists on goethite that is capable of sustaining conduction, which facilitates complete recrystallization and isotopic exchange.

Received: October 7, 2014



ACS Publications

© XXXX American Chemical Society

A

DOI: 10.1021/ct500891a
J. Chem. Theory Comput. XXXX, XXX, XXX–XXX

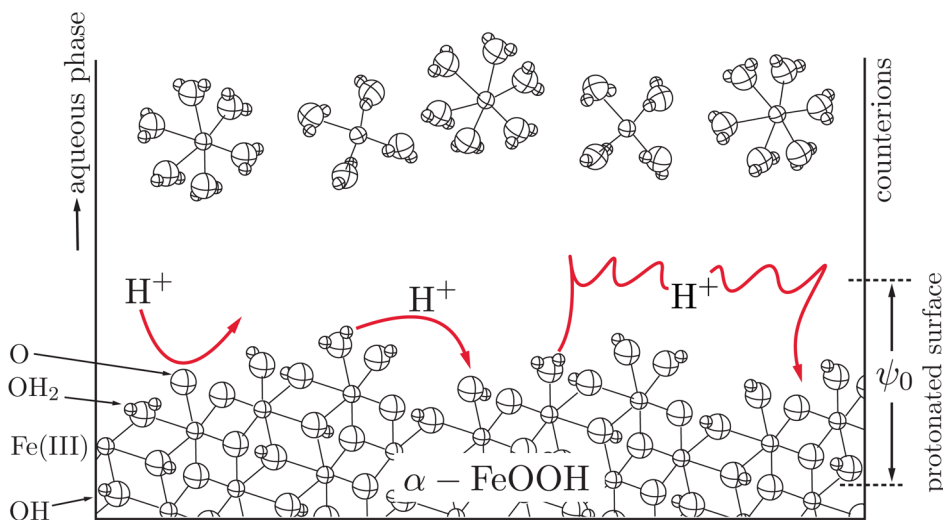


Figure 1. Schematic illustration of spontaneous proton transfer at the charged goethite (α -FeOOH)/electrolyte interface. The surface charge is formed due to the protonation of the surface hydroxy groups (FeO, FeOH, FeOH₂). This surface charge is neutralized by the non-specifically surface-bound counterions that are localized in the outer Helmholtz plane or in the diffuse layer.

We hypothesize that because of fluctuations in protonation/deprotonation states of surfaces, an instantaneous potential bias across goethite/water interfaces will exist (Figure 1). Aspects of proton dynamics at these interfaces have been addressed previously and are relevant. For example, proton conductivity at hydrated metal oxide surfaces seems to have a much faster response than electronic/protonic conductivity through the solid.^{14,21} Also, close vicinity of protons at surface sites are important for the dynamics through mutual interaction. Strong horizontal hydrogen bonds between neighboring surface groups favors hopping between sites, and they may suppress H⁺ diffusion above the surface.²¹ On the other hand, weak hydrogen bonds between water in the first solvation layer²² may facilitate proton diffusion above the surface, mediated by the interfacial water molecules. We furthermore posit that if these collective protonation/deprotonation fluctuations have prominent frequencies that are slower than interfacial ET and small polaron hopping rates, the dynamics of protonation/deprotonation will influence ET and polaronic conduction in the recrystallization of goethite by Fe(II). In such a case, electrons on adsorbed donor Fe(II) after interfacial ET on the goethite near-surface Fe sublattice will “feel” the presence of a fluctuating electrical bias arising from the dynamics of protonation/deprotonation reactions at the surface and tend to migrate accordingly. We propose that a transient imbalance in net surface charge will always exist between crystallographically identical and distinct crystal faces on goethite, likely coupled to their redox reactivity, conceptually consistent with the available experimental results.^{12,23–25}

In this report, using atomistic simulations, we provide the first physical evidence of the spontaneously arising and fluctuating potential biases at goethite/water interfaces at different pH values.¹² In particular, we analyze the frequency and amplitude of the fluctuations, and the magnitude of the corresponding time-averaged surface potential gradient, and discuss how these characteristics can influence interfacial ET and bias the migration of small polarons in the iron oxide lattice.^{10,26–28} The computational methods developed and used for this purpose are unique.

2. THEORY, COMPUTATION, AND ANALYTICAL METHODOLOGIES

Numerous computational methodologies for charged metal oxides have been published (see, for instance, refs 30–36); however, there are very few atomistic modeling studies that implicitly take into account a dynamical aspect of the pH-dependent surface protonation.^{23,32–34,37–42} Although protonation can be easily implemented in the Monte Carlo (MC) scheme,^{23,37,38} molecular dynamics (MD) simulations are typically carried out with unchanged chemical identity of surface species (with a few notable exceptions^{32–34}). Here, we implemented the MD algorithm that allow the protonable sites to adjust on-the-fly their H⁺ population, following the principles of the constant-pH molecular dynamics (cpHMD) as it was developed for biological systems.^{43–48} The discrete protonation algorithm, as used in this report, the system explores both the protonation space (MC) and configurational space (MD). This strategy is often referred to as the hybrid MD-MC scheme, and it involves sequential switching between the stochastic attempts to change the protonation state (MC) and classical time evolution (MD).

There are, however, two problematic issues in successful cpHMD application to metal oxides. The first one is the question of frequency in updating the protonation state, and the second is the question of how long the system should evolve in configurational space to reach thermal equilibrium. The latter also raises a question of the solvent relaxation and proton residence times. All these issues are typically addressed by *ab initio* MD.^{49–51}

Mechanism and Time Scale of Proton Hopping.

cpHMD methods alone are unable to reveal the proton hopping mechanisms nor proton-transfer time scales; therefore, these aspects are neglected in this report as we focus primarily on modeling the average potential and fluctuations in protonation end-states at dynamic equilibrium with constant pH solutions. What is more, the frequency of stochastic titration and the span of the MD interval need to be parametrized *a priori* in the cpHMD modeling. Some independent insight is needed as well, such as through *ab initio* MD studies of proton in aqueous solution (hopping pathway, rates).^{45,47–57}

Extensions of this topic and methods to hydrated metal oxide surfaces are relatively few,^{39–42,58,59} mostly due to overwhelming computational cost. Recently, Tocci and Michaelides³⁹ found that the rate of proton hopping and the height of the hopping energy barrier at ZnO surfaces depend on the interfacial water content. Their studies suggested that proton transfer becomes energetically more favorable as the water coverage increases.³⁹ More specifically, they found that the presence of the second layer of water molecules at the ZnO(10̄10) crystal face deceases the energy barrier for H⁺ hopping by half (from 6.4 to 2.8 k_{BT} units).³⁹ It has also been reported that the experimentally determined rate of proton transfer is faster (average hopping time \sim 20 fs)³⁹ at the hydrated ZnO surface than in pure water (<100 fs).⁶⁰

Merte et al.⁶¹ showed that proton hopping at the (111) FeO crystal face is indeed also facilitated by the presence of water. Their experimental results suggest that H⁺ moves on the surface in a concerted way with periods of intense coupled hopping and periods of rest, similar to the *ab initio* studies of proton hopping in pure water.^{49,50}

In the context of the proton hopping rate being strongly affected by water layers,^{39,61} it is worth mentioning that previously reported MD studies showed that apparently similar water layers at various crystal faces of iron oxides differ significantly in the number, type, and strength of the hydrogen bonds formed between the water molecules and surface hydroxy groups, and likewise also the water dipole orientation in the first solvation shell.^{22,35,62} Consequently, one may expect that proton hopping dynamics differ significantly at various crystal faces.

Implementation for Goethite Nanoparticles. A cpHMD scheme was successfully implemented for model goethite nanoparticles in aqueous solution. We started by constructing a charge-neutral nanoparticle (Figure 2), with surface protons distributed according to each surface site proton affinity as predicted by the multisite SCM.⁵ That is, the probability of oxygen protonation is proportional to the proton affinity constant estimated by Venema et al.,⁵ and it is assigned to each site based on the surface oxygen coordination. The nanoparticle was designed to be consistent with the atom-exchange experiments mentioned above.¹⁰ We used periodic boundary conditions, for which any density waves with length greater than the size of the computational cell are suppressed.⁶³ For this reason, one has to use the relatively large simulation box to avoid any long-range induced electrostatic coupling of the nanoparticle with its periodic image that may produce artificially correlated fluctuations. The model nanoparticle size was thus necessarily smaller than the experimental ones, because of the high computational expense. We selected nanoparticle faces to be the same crystal (110) faces that dominate the atom-exchange experiments with goethite nanorods,¹⁰ truncated by (001) end faces. Despite the fact that goethite crystals are currently described within the *Pnma* space group,²⁹ we used the older notation of the *Pbnm* space group to remain consistent with work by Handler et al.¹⁰ We ensured charge neutrality of separate crystal faces (i.e., $\sigma_0(hkl) = 0$ for $hkl = 001, 00\bar{1}, 110, \bar{1}10, \bar{1}\bar{1}0, 1\bar{1}0$). The charge-neutral nanoparticle was considered as a reference, that is, the particle at the pH near the PZC.

To model the spontaneously arising time-dependent voltage drop due to the protonation imbalance among nanoparticle faces, we imposed proton excess ($+\Delta H^+$) or depletion ($-\Delta H^+$) by randomly protonating/deprotonating sites with highest/lowest proton affinities (as predicted by Venema et al.⁵). In order to model the pH dependence, we imposed lower or higher

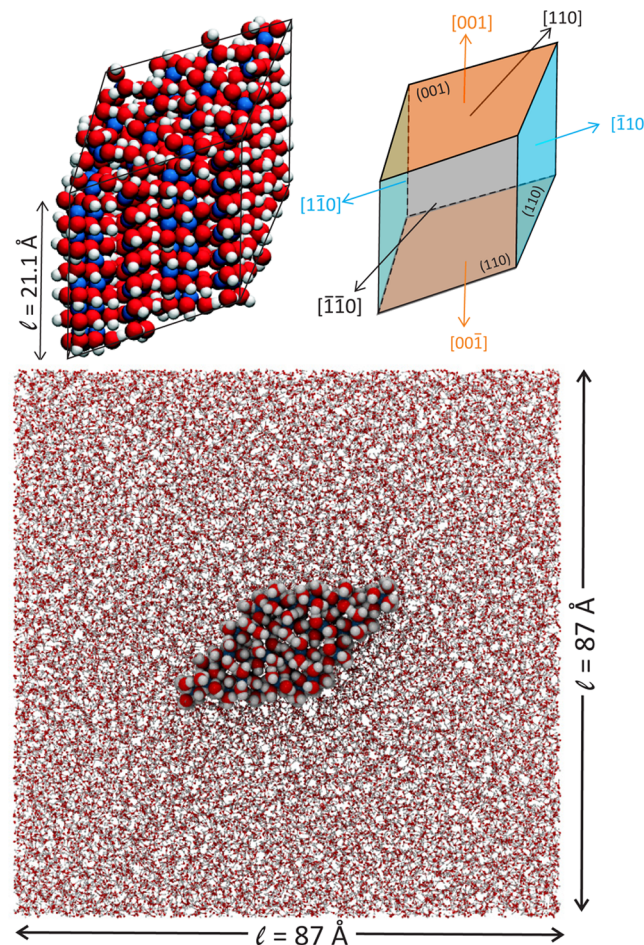


Figure 2. Hydrated goethite (α -FeOOH) nanoparticle used in modeling the transient electrostatic properties (faces exposed by particle are indicated by the directions of perpendicular axes and faces). The crystal faces and directions are expressed in the *Pbnm* space group, for consistency of notation with Handler et al.¹⁰ The conversion between the *Pnma* and *Pbnm* space groups is straightforward: $Pbnm(110) = Pnma(101)$, $Pbnm(001) = Pnma(100)$.²⁹ The morphology of the goethite nanoparticle resembles the morphology of the goethite nanorods and microrods used in contemporary experimental studies.¹⁰

number of surface protons on the whole nanoparticle as compared to the proton population in the charge-neutral case. Because faces are in direct electrostatic contact due to their close proximity, the protons population at each crystal face quickly relaxes in response to the properties of the other faces.

We used the replica-exchange cpHMD approach to model the dynamical proton redistribution. The algorithm implemented here is based on the cpHMD algorithm that alternates the MC sampling of the protonation space and MD sampling of configuration space.^{43,44} To overcome the possible system trapping in local minima, we followed the pH-based replica-exchange approach introduced by Roitberg's group.^{64–66} Our cpHMD implementation (Figure 3) is inspired by their work.^{65,67–70} We also used simulated annealing⁷¹ procedure to avoid extended system trapping due to cooperative effects and strong electrostatic correlation among the vicinal surface sites. We used the Smooth Particle Mesh Ewald⁷² summation algorithm for modeling the long-range electrostatic interactions in a periodically replicated system (cubic boundary conditions). In the MC part, we accept a new configuration based on the Metropolis–Hastings⁷³ weighting function. The time evolution

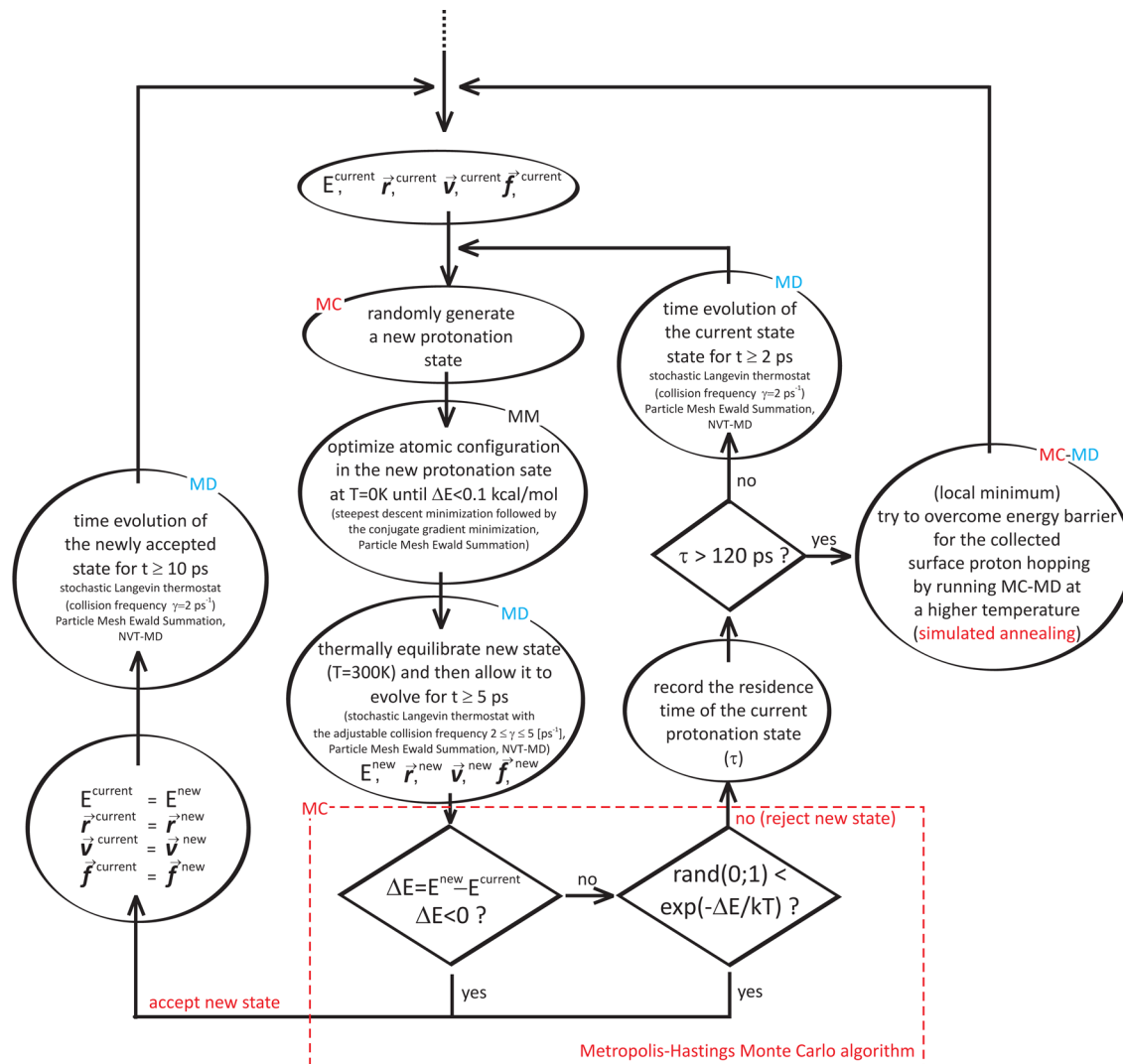


Figure 3. Algorithm for constant surface charge molecular dynamics/Monte Carlo simulations of the overall charge-neutral goethite nanoparticle with simulated annealing for escaping from energetic traps (metastable protonation state).

was obtained by using the velocity Verlet integrator⁶³ with time step $\delta t = 0.001$ ps. The MD of the newly accepted protonation state was carried out for 10 ps, before attempting to change the protonation state in the MC part. Our time intervals for the MD and frequency of attempt to update the protonation state are dictated by the AIMD results⁵⁰ that suggest the concerted proton hopping occurs within 1–5 ps. The goethite and goethite/water interaction parameters were described by the same force-field as in our previous work,⁷⁴ except that water was represented by the rigid SPC/E model^{75,76} for simplicity. It is worth mentioning, that we used the rigid, non-polarizable and non-dissociable water model to significantly simplify computations, focusing only on the change in protonation state of the goethite surface. By using SPC/E model we are unable to follow the proton fate in solution, and its actual water-mediated hopping pathway from one site to the other. This simplification is motivated by the enormous complexity associated with taking into account protonation states of all water molecules. The polarization of the oxide oxygen atoms is, however, included as before.⁷⁴ We carried out our cpHMD simulations in a parallel fashion (Message Passing Interface library) for 30–50 ns.

We first prepared a charge-neutral nanoparticle, and then we immersed it in a bulk of the SPC/E water molecules,^{75,76}

minimizing the initial atomic positions using the steepest descent algorithm.⁷⁷ In the following step, we heated the system to 298 K (Langevin thermostat^{78,79} with collision frequency $\gamma = 2 \text{ ps}^{-1}$, NVT ensemble) for 0.2 ns. Finally, we optimized the computational cell density by running the NPT molecular dynamics for 4 ns (Berendsen thermostat–barostat⁸⁰). The cell prepared in such way, was used as an input for all reported cpHMD simulations.

Protons accumulation at the charged oxide surface ($[\text{H}^+]_{\text{surface}}$) is determined by the bulk H^+ ion concentration (pH = $-\log [\text{H}^+]_{\text{bulk}}$) and surface electrostatic potential (ψ_0) according to the Boltzmann-type equation:³⁸

$$[\text{H}^+]_{\text{surface}} = [\text{H}^+]_{\text{bulk}} \exp\left(-\frac{e\psi_0}{k_B T}\right) \quad (1)$$

A simple rearrangement leads to the following definition of ψ_0 :

$$\psi_0(\text{pH}) = \frac{k_B T}{e} \ln \frac{[\text{H}^+]_{\text{bulk}}}{[\text{H}^+]_{\text{surface}}} \quad (2)$$

In our modeling we constrained only surface charge (not the bulk pH), but we can still define the transient surface

potential gradient between two crystal faces i and j via eq 2 as follows:

$$\Delta\psi_{0(ij)} = \psi_{0,i} - \psi_{0,j} = \frac{k_B T}{e} \ln \frac{[\text{H}^+]_j^{\text{surface}}}{[\text{H}^+]_i^{\text{surface}}} \quad (3)$$

where surface proton accumulation (surface concentration) is given by the fraction of the number of the surface-bound protons $N_{\text{H}^+,i}$ to the given surface area A_i . In counting surface protons we take into account the singly ($\equiv\text{FeOH}$) and doubly ($\equiv\text{FeOH}_2$) protonated sites, that is, $N_{\text{H}^+,i} = N_{\text{FeOH},i} + 2N_{\text{FeOH}_2,i}$.

Configuration Sampling. As pointed out by Roitberg and co-workers,^{65,67,70} hybrid MC-MD cpHMD simulations suffer frequently from an inadequate sampling of the configuration and protonation spaces due to system trapping in local energetic minima (see ref 65 and references within). To avoid energetic trapping, we implemented the replica-exchange algorithm following Roitberg and co-workers.^{65,67,70} Specifically, if attempts to switch protonation state are continuously rejected (>120 ps), then we switch to simulated annealing (SA) exploration of configuration space at temperature T^{SA} , defined by the average of experienced energy barriers ($\Delta\mathcal{H} = \mathcal{H}^{\text{new}} - \mathcal{H}^{\text{current}} > 0$) in a few (N_f) previously unsuccessful attempts to change the protonation state:

$$T^{\text{SA}} = \frac{2}{3N_f k_B} \sum_{i=1}^{N_f} (\mathcal{H}_i^{\text{new}} - \mathcal{H}_i^{\text{current}}) \quad (4)$$

The primary system and its replica were brought to the desired T^{SA} temperature by gradually heating in 10 subsequent steps. In each step we simulated the system until it reached a thermal equilibrium. Simulated annealing was carried out in the NVT ensemble with restrained core of nanoparticle to avoid dissolution/structural reconstruction triggered by any non-uniform density fluctuations expected in the NPT ensemble or at higher temperature.

Frequency Analysis of Surface Potential Fluctuations. Analysis of the frequencies of cpHMD-based surface potential fluctuations was performed by Fourier transform (FT) of the time series data from 0 to 30 ns (Figures 4 and 5) into the frequency domain. Due to MC-MD coupling, surface potential fluctuations calculated with this approach are recorded with non-uniform time spacing, with a minimum spacing of 0.5 ps and maximum spacing of 7 ps. Therefore, time-series data were bin-averaged using a bin width of 30 ps prior to FT (1000 bins), remedying the non-uniform time spacing at the expense of limiting maximum observable frequency to 3.33×10^{10} Hz. Additionally the data were zero-padded to decrease spacing between frequencies in the FT power spectrum in order to make minima and maxima more apparent without affecting peak positions or line width ("upsampling", ref 81). Note that 30 ps time spacing corresponds to 3.33×10^7 Hz frequency spacing. The data were padded with zeroes to reduce the frequency interval to 2×10^6 Hz. Following data processing and FT, the frequency domain of surface potential fluctuations spans 3.33×10^7 to 3.33×10^{10} Hz, with a spacing of 2×10^6 Hz.

3. RESULTS AND DISCUSSION

Given that the goal of our simulations is to understand the magnitude and frequency of protonation-based surface potential fluctuations, and to relate this to prospective coupling to polaronic ET rates in the surface, we first briefly discuss physical limitations with respect to this coupling. The differences between

the mean surface potential $\langle\psi_0\rangle$ between two crystal faces of interest is taken as the persistent average bias voltage between those two faces. We intend to understand frequencies of these protonation-based surface potential fluctuations and compare them to estimates of electron hopping rates in the goethite solid, to establish whether or not these fluctuations can influence electron migration. Because the elementary protonation/deprotonation frequencies in our cpHMD model is based on physically realistic frequencies of H^+ transport (1–5 ps), the frequency information in the time-series data are physical frequencies, as opposed to arbitrary ones. We thus analyzed these time-series data by Fourier transform to get the frequency domain and the power spectrum to determine if surface potential fluctuation rates are competitive with hopping rates of electron–small polaron charge carriers, determined elsewhere to be on the order of 10^9 Hz.¹⁶

For protonation-based surface potential fluctuations to influence charge carrier migration, we assume their magnitude must exceed the normal voltage fluctuations of charge carriers at equilibrium, at frequencies equal to or slower than polaronic hopping rates. The fluctuation–dissipation theory connects the potential fluctuations with the local resistivity and potential fluctuation frequency as proposed by Johnson⁸² and Nyquist.⁸³ According to this theory, the naturally arising positional fluctuations of the charge carriers results in a subtle voltage variance that is referred as the Johnson–Nyquist noise or the white resistor noise ($\delta\psi = \langle\psi^2\rangle^{1/2} = (4k_B T R)^{1/2}$, where R is the resistor value).^{82–85} This voltage drop is typically in order of a few μV , in the case of the electron thermal agitation,^{82,83} and probably even smaller in the case of protonic conductors.⁸⁶ In goethite at room temperature the Johnson–Nyquist noise is approximately $0.51 \mu\text{V}$. If the surface potential fluctuations do not exceed this value then this perturbation is subsumed into the spontaneous electronic noise and no coupling to charge carrier migration can be expected.

In Figures 4 and 5 we show calculated time-dependent fluctuations of the potential gradient between symmetrical opposing faces (Figure 5) and non-equivalent edge-sharing faces (Figure 5). Because the symmetrical, opposing faces have exactly the same characteristics (surface site type and density, site stoichiometry) the average potential bias difference between such faces is always zero. From Figure 4 it can be seen that the range of potential gradient fluctuation decreases with increasing surface area of the exposed crystal faces ($\Delta\psi_0^{\text{max}}: (110)/(\bar{1}\bar{1}0) < (\bar{1}10)/(1\bar{1}0) < (001)/(00\bar{1})$). This can be expected, because the smaller the surface area the larger perturbation that is caused by changing the protonation state of only one surface site. A similar conclusion can be drawn on the basis of Figure 5: namely, for the crystal faces possessing a similar number of surface sites (and similar surface area) the potential gradient is very small and it fluctuates around zero (Figure 5a). However, if the faces differ significantly in surface area, than a non-vanishing potential gradient proportional to the surface area difference is formed. For instance, as can be seen in Figure 5b,c, $\langle\Delta\psi_0 = \psi_0(1\bar{1}0) - \psi(\bar{1}10)\rangle$ is around -20 mV and $\langle\Delta\psi_0 = \psi_0(\bar{1}10) - \psi(001)\rangle$ is about -25 mV .

It thus appears that the potential gradient between various crystal faces becomes more relevant as a driving force for electron transfer as the nanoparticle size decreases (i.e., $\Delta\psi_0$ particle size-dependent). Another important consequence is that the average absolute potential gradient between faces ($\langle|\Delta\psi_0|\rangle$) increases as the ratio of the surface areas or ratio of the number of exposed active surface sites of both faces increases. This means that

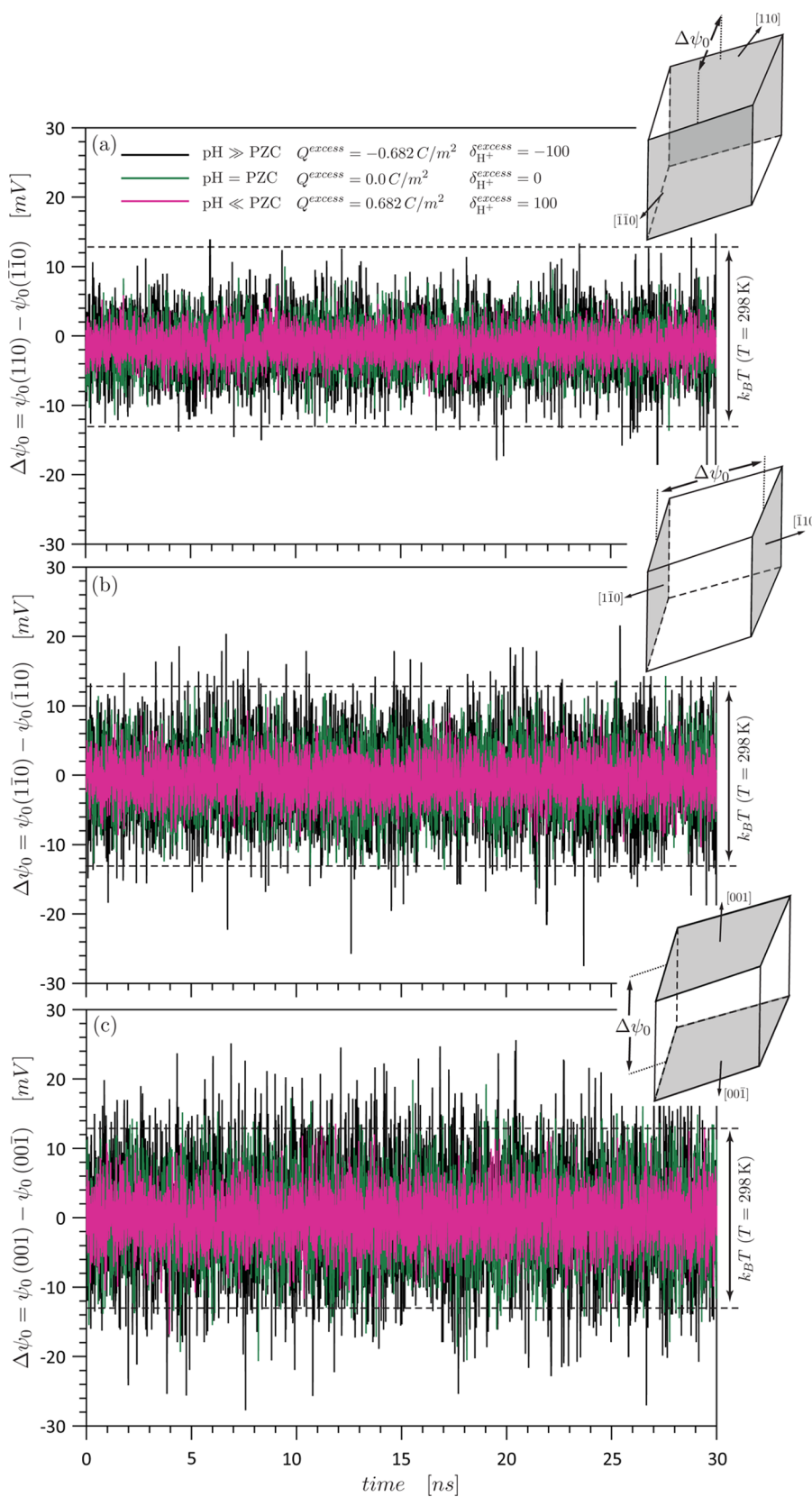


Figure 4. Time evolution of the surface potential gradient (voltage bias) between mirrored crystal faces (i.e., symmetrical faces) exposed by the goethite nanoparticle. The surface area and the number of exposed protonable groups decrease in a sequence: (a) $[\bar{1}\bar{1}0]/[110] >$ (b) $[\bar{1}10]/[1\bar{1}0] \geq$ (c) $[001]/[00\bar{1}]$.

particle morphology affects directionality of the potential gradient, and consequently the direction of any gradient-initiated counter-process (i.e., process acting against $\Delta\psi_0$).

In Figure 6, the power spectrum of surface potential fluctuation frequencies across equivalent faces determined by Fourier transform are presented. The highest-amplitude peaks are within

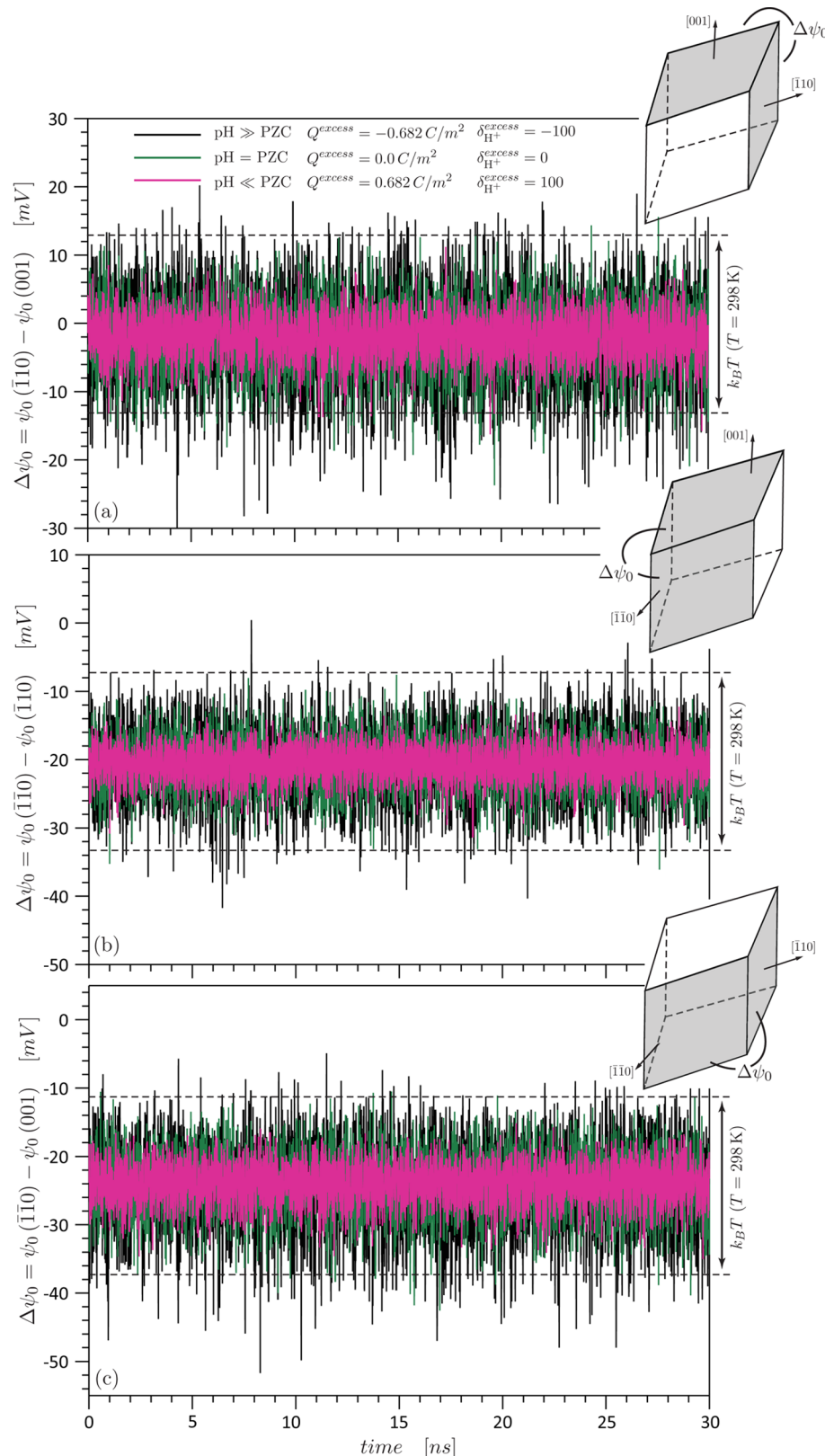


Figure 5. Time evolution of the surface potential gradient (voltage bias) between edge-sharing crystal faces (i.e., asymmetrical faces) exposed by the goethite nanoparticle.

the low-frequency portion of the analyzed frequency range, and are representative of the dominant collective motion associated with the respective potential fluctuations. Regardless of the sign of the time-averaged surface potential, the predominant frequency is on

the order of 10^7 Hz, a value 2 orders of magnitude slower than the rate of electron–small polaron hopping in goethite.¹⁶

Our simulations thus predict that non-negligible, directional electrostatic biases exist between various exposed crystal faces of

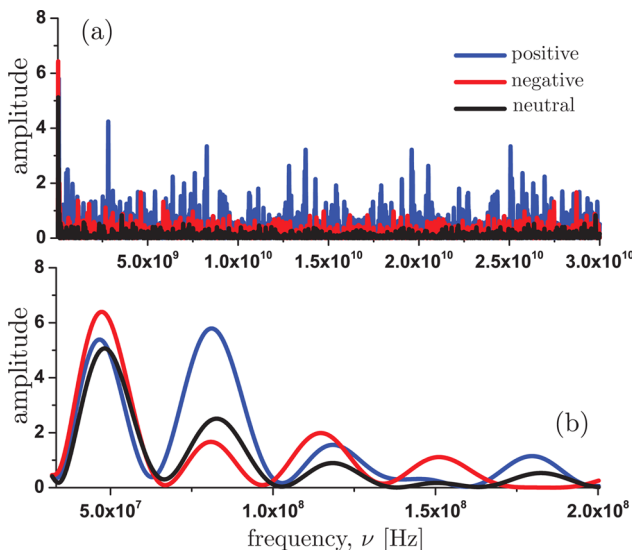


Figure 6. Fourier-transform of time-dependent potential gradient between symmetrical faces at different net charges: (top) full power spectrum; (bottom) low-frequency power spectrum. The low-frequency FT power spectrum shows that the dominant (highest-amplitude) frequencies are on the order of 10^7 Hz, regardless of the sign of the time-averaged surface potential (4.6 and 8.2×10^7 Hz for positive sign and 4.8×10^7 Hz for negative sign).

goethite particles, their magnitude and direction depends on how much the exposed faces differ in terms of area and surface site density. In our simulation size-regime, areas of exposed surfaces are very small, allowing almost instantaneous electrostatic connection via surface H^+ dynamics. On the one hand, small areas of exposed surfaces result in small potential biases (k_{BT}) and high-frequencies of $\Delta\psi_0$ fluctuation (4.5×10^7 Hz). On the other hand, even for such a small particle potential gradient between any two faces, it is still over 10^3 times larger in magnitude than Johnson–Nyquist resistive-noise and possesses lowest-frequency fluctuations about 10^2 times lower than frequency of polaron hopping in goethite. Therefore, our simulations support the notion of surface H^+ -dynamics as a driving force for surface conductivity of goethite particles.

4. CONCLUSIONS

A replica-exchange constant-pH molecular dynamics simulation approach for protonation-based surface potential dynamics on metal oxide nanoparticles has been presented. The approach represents an advance over macroscopic equilibrium thermodynamics tools such as surface complexation modeling, in that it takes into account the microscopic details of the surface structure and hydration, both the equilibrium and non-equilibrium fluctuations in surface charge density, and collective electrostatic interactions of all relevant species at the atomic level. The approach has specifically been applied to predict the magnitude and frequency of surface potential fluctuations on nanoparticles of goethite, in the context of understanding the extent to which these dynamical interactions can couple to electron migration in the nanoparticles.

Our simulations show that charged surfaces exposed by the same particle are electronically coupled via surface H^+ dynamics. We found that any change in protonation state at one face is quickly propagated to the others via the instantaneous potential bias. Although calculated potential gradients are small, they are still orders of magnitude larger than resistive noise

in goethite, and are expected to be larger if larger particles are considered.

To reach a gradient-free equilibrium condition, the transient potential bias formed between edge-sharing faces of goethite nanoparticles has to vanish. It may be consumed to facilitate the subsurface electron hopping, or to induce face-specific dissolution/precipitation at the nanoparticle surface. The former is believed to play a crucial role in iron isotopic exchange at the goethite/aqueous Fe(II) electrolyte phase.¹⁰ The latter was proposed as an explanation of the link surface–bulk reactivity of hematite single crystals.¹² As is the case for protein-based proton pumps, the interplay between electric field fluctuations and interfacial electron-transfer dynamics has been a topic of intense research for solid/electrolyte interfaces.^{87,88}

The question of whether the transient potential gradients between exposed crystal faces of goethite nanoparticle are capable of sustaining bulk conduction is still very much an open one. We hope that this report bridges the gap in our understanding of metal oxide nanoelectrostatics by providing the first atomistic proof that indeed the dynamical surface protonation generates a significant potential bias, whose magnitude exceeds the naturally arising Johnson–Nyquist fluctuation.

■ AUTHOR INFORMATION

Corresponding Author

*Phone: +48 22 343 3258. E-mail: zarzycki.piotrek@gmail.com.

Notes

The authors declare no competing financial interest.

■ ACKNOWLEDGMENTS

This work was supported by the Ministry of Science and Higher Education (Poland), grant IP2012 059872, and by the Geosciences Research Program at Pacific Northwest National Laboratory (PNNL), sponsored by the U.S. Department of Energy (DOE), Office of Science, Office of Basic Energy Sciences (BES), Division of Chemical Sciences, Geosciences & Biosciences. A portion of this research was performed using EMSL, a national scientific user facility sponsored by the DOE's Office of Biological and Environmental Research and located at PNNL. PNNL is a multiprogram national laboratory operated for DOE by Battelle.

■ REFERENCES

- (1) Brown, G. E.; Henrich, V. E.; Casey, W. H.; Clark, D. L.; Eggleston, C.; Felmy, A.; Goodman, D. W.; Grätzel, M.; Maciel, G.; McCarthy, M. I.; Nealson, K. H.; Sverjensky, D. A.; Toney, M. F.; Zachara, J. M. Metal Oxide Surfaces and Their Interactions with Aqueous Solutions and Microbial Organisms. *Chem. Rev.* **1999**, *99*, 77–174.
- (2) Braunschweig, J.; Bosch, J.; Meckenstock, R. U. Iron Oxide Nanoparticles in Geomicrobiology: from Biogeochemistry to Bio-remediation. *New Biotechnol.* **2013**, *1*–10.
- (3) Hiemstra, T.; Venema, P.; van Riemsdijk, W. Intrinsic Proton Affinity of Reactive Surface Groups of Metal (Hydr)oxides: The Bond Valence Principle. *J. Colloid Interface Sci.* **1996**, *184*, 680–692.
- (4) Yates, D. E.; Levine, S.; Healy, T. W. Site-Binding Model of the Electrical Double Layer at the Oxide/Water Interface. *J. Chem. Soc., Faraday Trans. 1* **1974**, *70*, 1807.
- (5) Venema, P.; Hiemstra, T.; Weidler, P. G.; van Riemsdijk, W. H. Intrinsic Proton Affinity of Reactive Surface Groups of Metal (Hydr)oxides: Application to Iron (Hydr)oxides. *J. Colloid Interface Sci.* **1997**, *198*, 282–295.
- (6) Scherer, M. M.; Balko, B. A.; Tratnyek, P. G. *Mineral-Water Interfacial Reactions*; ACS Symposium Series 715; American Chemical Society: Washington, DC, 1999; 301–322.

- (7) Williams, A. G. B.; Scherer, M. M. Spectroscopic Evidence for Fe(II)-Fe(III) Electron Transfer at the Iron Oxide-Water Interface. *Environ. Sci. Technol.* **2004**, *38*, 4782–4790.
- (8) Beard, B. L.; Handler, R. M.; Scherer, M. M.; Wu, L.; Czaja, A. D.; Heimann, A.; Johnson, C. M. Iron Isotope Fractionation between Aqueous Ferrous Iron and Goethite. *Earth Planet. Sci. Lett.* **2010**, *295*, 241–250.
- (9) Cwiertny, D. M.; Handler, R. M.; Schaefer, M. V.; Grassian, V. H.; Scherer, M. M. Interpreting Nanoscale Size-Effects in Aggregated Fe-Oxide Suspensions: Reaction of Fe(II) with Goethite. *Geochim. Cosmochim. Acta* **2008**, *72*, 1365–1380.
- (10) Handler, R. M.; Beard, B. L.; Johnson, C. M.; Scherer, M. M. Atom Exchange between Aqueous Fe(II) and Goethite: An Fe Isotope Tracer Study. *Environ. Sci. Technol.* **2009**, *43*, 1102–1107.
- (11) Latta, D. E.; Gorski, C. A.; Scherer, M. M. Influence of Fe²⁺-Catalysed Iron Oxide Recrystallization on Metal Cycling. *Biochem. Soc. Trans.* **2012**, *40*, 1191–1197.
- (12) Yanina, S. V.; Rosso, K. M. Linked Reactivity at Mineral-Water Interfaces Through Bulk Crystal Conduction. *Science* **2008**, *320*, 218–222.
- (13) Guskos, N.; Papadopoulos, G. J.; Likodimos, V.; Patapis, S.; Yarmis, D.; Przepiera, A.; Przepiera, K.; Majszczyk, J.; Typek, J.; Wabia, M.; Aidinis, K.; Drazek, Z. Photoacoustic, EPR and Electrical Conductivity Investigations of three Synthetic Mineral Pigments: Hematite, Goethite and Magnetite. *Mater. Res. Bull.* **2002**, *37*, 1051–1061.
- (14) Katz, J. E.; Zhang, X.; Attenkofer, K.; Chapman, K. W.; Frandsen, C.; Zarzycki, P.; Rosso, K. M.; Falcone, R. W.; Waychunas, G. A.; Gilbert, B. Electron Small Polarons and Their Mobility in Iron (Oxyhydr)oxide Nanoparticles. *Science* **2012**, *337*, 1200–1203.
- (15) Böttger, H., Bryksin, V. V. *Hopping Conduction in Solids*; Verlag: Weinheim, 1985; pp 51–85.
- (16) Alexandrov, V.; Rosso, K. M. Electron Transport in Pure and Substituted Iron Oxyhydroxides by Small-Polaron Migration. *J. Chem. Phys.* **2014**, *140*, 234701.
- (17) Rosso, K. M.; Smith, D. M. A.; Dupuis, M. An ab Initio Model of Electron Transport in Hematite (α -Fe₂O₃) Basal Planes. *J. Chem. Phys.* **2003**, *118*, 6455.
- (18) Iordanova, N.; Dupuis, M.; Rosso, K. M. Charge Transport in Metal Oxides: A Theoretical Study of Hematite α -Fe₂O₃. *J. Chem. Phys.* **2005**, *122*, 144305.
- (19) Handler, R. M.; Friedrich, A. J.; Johnson, C. M.; Rosso, K. M.; Beard, B. L.; Wang, C.; Latta, D. E.; Neumann, A.; Pasakarnis, T.; Premaratne, W. A. P. J.; Scherer, M. M. Fe(II)-Catalyzed Recrystallization of Goethite Revisited. *Environ. Sci. Technol.* **2014**, *48*, 11302–11311.
- (20) Friedrich, A. J.; Beard, B. L.; Reddy, T. R.; Scherer, M. M.; Johnson, C. M. Iron Isotope Fractionation Between Aqueous Fe(II) and Goethite Revisited: New Insights Based on a Multi-Direction Approach to Equilibrium and Isotopic Exchange Rate Modification. *Geochim. Cosmochim. Acta* **2014**, *139*, 383–398.
- (21) Kreuer, K.-D. Proton Conductivity: Materials and Applications. *Chem. Mater.* **1996**, *8*, 610–641.
- (22) Boily, J.-F. Water Structure and Hydrogen Bonding at Goethite/Water Interfaces: Implications for Proton Affinities. *J. Phys. Chem. C* **2012**, *116*, 4714–4724.
- (23) Zarzycki, P.; Chatman, S.; Preočanin, T.; Rosso, K. M. Electrostatic Potential of Specific Mineral Faces. *Langmuir* **2011**, *27*, 7986–7990.
- (24) Chatman, S.; Zarzycki, P.; Rosso, K. M. Surface Potentials of (001), (012), (113) Hematite (α -Fe₂O₃) Crystal Faces in Aqueous Solution. *Phys. Chem. Chem. Phys.* **2013**, *15*, 13911.
- (25) Chatman, S.; Zarzycki, P.; Preočanin, T.; Rosso, K. M. Effect of Surface Site Interactions on Potentiometric Titration of Hematite (α -Fe₂O₃) crystal faces. *J. Colloid Interface Sci.* **2013**, *391*, 125–134.
- (26) Gorski, C. A.; Scherer, M. M. *Fe²⁺ Sorption at the Fe Oxide-Water Interface: A Revised Conceptual Framework*; American Chemical Society: Washington, DC, 2011; pp 315–343.
- (27) Friedrich, A. J.; Scherer, M. M.; Bachman, J. E.; Engelhard, M. H.; Rapponotti, B. W.; Catalano, J. G. Inhibition of Trace Element Release During Fe(II)-Activated Recrystallization of Al-, Cr-, and Sn-Substituted Goethite and Hematite. *Environ. Sci. Technol.* **2012**, *46*, 10031–10039.
- (28) Friedrich, A. J.; Catalano, J. G. Controls on Fe(II)-Activated Trace Element Release from Goethite and Hematite. *Environ. Sci. Technol.* **2012**, *46*, 1519–1526.
- (29) Cornell, R. M.; Schwertmann, U. *The Iron Oxide. Structure, Properties, Reactions, Occurrence and Uses*; Wiley: Weinheim, 2003; pp 9–38.
- (30) Borkovec, M. Origin of 1-pK and 2-pK Models for Ionizable Water-Solid Interfaces. *Langmuir* **1997**, *13*, 2608–2613.
- (31) Kerisit, S.; Rosso, K. M. Computer Simulation of Electron Transfer at Hematite Surfaces. *Geochim. Cosmochim. Acta* **2006**, *70*, 1888–1903.
- (32) Rustad, J. R.; Hay, B. P. A Molecular Dynamics Study of Solvated Orthosilicic Acid and Orthosilicate Anion using Parametrized Potentials. *Geochim. Cosmochim. Acta* **1995**, *59*, 1251–1257.
- (33) Rustad, J. R.; Wasserman, E.; Felmy, A. R.; Wilke, C. Molecular Dynamics Study of Proton Binding to Silica Surfaces. *J. Colloid Interface Sci.* **1997**, *198*, 119–129.
- (34) Rustad, J. R.; Felmy, A. R. The Influence of Edge Sites on the Development of Surface Charge on Goethite Nanoparticles: A Molecular Dynamics Investigation. *Geochim. Cosmochim. Acta* **2005**, *69*, 1405–1411.
- (35) Kerisit, S. Water Structure at Hematite-Water Interfaces. *Geochim. Cosmochim. Acta* **2011**, *75*, 2043–2061.
- (36) Halley, J. W.; Rustad, J. R.; Rahman, A. A Polarizable, Dissociating Molecular Dynamics Model for Liquid Water. *J. Chem. Phys.* **1993**, *98*, 4110.
- (37) Zarzycki, P. Comparison of the Monte Carlo Estimation of Surface Electrostatic Potential at the Hematite (0001)/Electrolyte Interface with the Experiment. *Appl. Surf. Sci.* **2007**, *253*, 7604–7612.
- (38) Zarzycki, P.; Rosso, M. K Nonlinear Response of the Surface Electrostatic Potential Formed at Metal Oxide/Electrolyte Interfaces. A Monte Carlo Simulation Study. *J. Colloid Interface Sci.* **2010**, *341*, 143–152.
- (39) Tocci, G.; Michaelides, A. Solvent-Induced Proton Hopping at a Water-Oxide Interface. *J. Phys. Chem. Lett.* **2014**, *4*, 474–480.
- (40) Gaigeot, M.-P.; Sprik, M.; Sulpizi, M. Oxide/water Interfaces: How the Surface Ehemistry Modifies Interfacial Water Properties. *J. Phys.: Condens. Matter* **2012**, *24*, 124106.
- (41) Tazi, S.; Rotenberg, B.; Salanne, M.; Sprik, M.; Sulpizi, M. Absolute Acidity of Clay Edge Sites from Ab-Initio Simulations. *Geochim. Cosmochim. Acta* **2012**, *94*, 1–11.
- (42) Liu, X.; Lu, X.; Sprik, M.; Cheng, J.; Meijer, E. J.; Wang, R. Acidity of Edge Surface Sites of Montmorillonite and Kaolinite. *Geochim. Cosmochim. Acta* **2013**, *117*, 180–190.
- (43) Mongan, J.; Case, D. A.; McCammon, J. A. Constant pH Molecular Dynamics in Generalized Born Implicit Solvent. *J. Comput. Chem.* **2004**, *25*, 2038–2048.
- (44) Mongan, J.; Case, D. A. Biomolecular Simulations at Constant pH. *Curr. Opin. Struct. Biol.* **2005**, *15*, 157–163.
- (45) Baptista, A. M.; Teixeira, V. H.; Soares, C. M. Constant-pH Molecular Dynamics using Stochastic Titration. *J. Chem. Phys.* **2002**, *117*, 4184–4200.
- (46) Dlugosz, M.; Antosiewicz, J.; Robertson, A. Constant-pH Molecular Dynamics Study of Protonation-Structure Relationship in a Heptapeptide Derived from Ovomucoid third Domain. *Phys. Rev. E* **2004**, *69*, 021915.
- (47) Dlugosz, M.; Antosiewicz, J. M. Constant-pH Molecular Dynamics Simulations: a Test Case of Succinic Acid. *Chem. Phys.* **2004**, *302*, 161–170.
- (48) Machuqueiro, M.; Baptista, A. M. Constant-pH Molecular Dynamics with Ionic Strength Effects: Protonation-Conformation Coupling in Decalsine. *J. Phys. Chem. B* **2006**, *110*, 2927–2933.
- (49) Hassanali, A.; Prakash, M. K.; Eshet, H.; Parrinello, M. On the Recombination of Hydronium and Hydroxide Ions in Water. *Proc. Natl. Acad. Sci. U.S.A.* **2011**, *108*, 20410–20415.

- (50) Hassanali, A.; Giberti, F.; Cuny, J.; Kühne, T. D.; Parrinello, M. Proton Transfer Through the Water Gossamer. *Proc. Natl. Acad. Sci. U.S.A.* **2013**, *110*, 13723–13728.
- (51) Geissler, P. L.; Dellago, C.; Chandler, D.; Hutter, J.; Parrinello, M. Autoionization in Liquid Water. *Science* **2001**, *291*, 2121–2124.
- (52) Marx, D.; Tuckerman, M. E.; Hutter, J.; Parrinello, M. The Nature of the Hydrated Excess Proton in Water. *Nature* **1999**, *397*, 601–604.
- (53) Ceriotti, M.; Cuny, J.; Parrinello, M.; Manolopoulos, D. E. Nuclear Quantum Effects and Hydrogen Bond Fluctuations in Water. *Proc. Natl. Acad. Sci. U.S.A.* **2013**, *110*, 15591–15596.
- (54) Tuckerman, M. E.; Marx, D.; Klein, M. L.; Parrinello, M. On the Quantum Nature of the Shared Proton in Hydrogen Bonds. *Science* **1997**, *275*, 817–820.
- (55) Lee, M. S.; Salsbury, F. R.; Brooks, C. L., III. Constant-pH Molecular Dynamics using Continuous Titration Coordinates. *Proteins* **2004**, *56*, 738–752.
- (56) Khandogin, J.; Brooks, C. L. Constant pH Molecular Dynamics with Proton Tautomerism. *Biophys. J.* **2005**, *89*, 141–157.
- (57) Marx, D. Proton Transfer 200 Years after von Grotthuss: Insights from Ab Initio Simulations. *ChemPhysChem* **2006**, *7*, 1848–1870.
- (58) Sulpizi, M.; Gaigeot, M.-P.; Sprik, M. The Silica-Water Interface: How the Silanols Determine the Surface Acidity and Modulate the Water Properties. *J. Chem. Theory Comput.* **2012**, *8*, 1037–1047.
- (59) Liu, X.; Cheng, J.; Sprik, M.; Lu, X.; Wang, R. Understanding Surface Acidity of Gibbsite with First Principles Molecular Dynamics Simulations. *Geochim. Cosmochim. Acta* **2013**, *120*, 487–495.
- (60) Woutersen, S.; Bakker, H. J. Ultrafast Vibrational and Structural Dynamics of the Proton in Liquid Water. *Phys. Rev. Lett.* **2006**, *96*, 138305.
- (61) Merte, L. R.; Peng, G.; Bechstein, R.; Rieboldt, F.; Farberow, C. A.; Grabow, L. C.; Kudernatsch, W.; Wendt, S.; Laegsgaard, E.; Mavrikakis, M.; Besenbacher, F. Water-Mediated Proton Hopping on an Iron Oxide Surface. *Science* **2012**, *336*, 889–893.
- (62) Song, X.; Boily, J.-F. Water Vapor Adsorption on Goethite. *Environ. Sci. Technol.* **2013**, *47*, 7171–7177.
- (63) Allen, M. P.; Tildesley, D. J. *Computer Simulation of Liquids*; Oxford University Press: Oxford, 1991; pp 78–81.
- (64) Itoh, S. G.; Damjanović, A.; Brooks, B. R. pH Replica-Exchange Method Based on Discrete Protonation States. *Proteins* **2011**, *79*, 3420–3436.
- (65) Sabri, D. D.; Meng, Y.; Roitberg, A. E. pH-Replica Exchange Molecular Dynamics in Proteins Using a Discrete Protonation Method. *J. Phys. Chem. B* **2012**, *116*, 8805–8811.
- (66) Wallace, J. A.; Shen, J. K. Continuous Constant pH Molecular Dynamics in Explicit Solvent with pH-Based Replica Exchange. *J. Chem. Theory Comput.* **2011**, *7*, 2617–2629.
- (67) Meng, Y.; Roitberg, A. E. Constant pH Replica Exchange Molecular Dynamics in Biomolecules Using a Discrete Protonation Model. *J. Chem. Theory Comput.* **2010**, *6*, 1401–1412.
- (68) Swails, J. M.; Roitberg, A. E. Enhancing Conformation and Protonation State Sampling of Hen Egg White Lysozyme Using pH Replica Exchange Molecular Dynamics. *J. Chem. Theory Comput.* **2012**, *8*, 4393–4404.
- (69) Sabri, D. D.; Roitberg, A. E. Optimization of Umbrella Sampling Replica Exchange Molecular Dynamics by Replica Positioning. *J. Chem. Theory Comput.* **2013**, *9*, 4692–4699.
- (70) Swails, J. M.; York, D. M.; Roitberg, A. E. Constant pH Replica Exchange Molecular Dynamics in Explicit Solvent Using Discrete Protonation States: Implementation, Testing, and Validation. *J. Chem. Theory Comput.* **2014**, *10*, 1341–1352.
- (71) Kirkpatrick, S.; Gelatt, C. D.; Vecchi, M. P. Optimization by Simulated Annealing. *Science* **1983**, *220*, 1–10.
- (72) Essmann, U.; Perera, L.; Berkowitz, M. L.; Darden, T.; Lee, H.; Pedersen, L. G. A Smooth Particle Mesh Ewald Method. *J. Chem. Phys.* **1995**, *103*, 8577.
- (73) Metropolis, N.; Rosenbluth, A. W.; Rosenbluth, M. N.; Teller, A. H.; Teller, E. Equation of State Calculations by Fast Computing Machines. *J. Chem. Phys.* **1953**, *21*, 1087.
- (74) Zarzycki, P.; Kerisit, S.; Rosso, K. Molecular Dynamics Study of the Interfacial Electron Transfer at the Goethite/Water Interface. *J. Phys. Chem. C* **2015**, *119* (6), 3111–3123.
- (75) Berendsen, H. J. C.; Grigera, J. R.; Straatsma, T. P. The Missing Term in Effective Pair Potentials. *J. Phys. Chem.* **1987**, *91*, 6269–6271.
- (76) Kusalik, P. G.; Svishchev, I. M. The Spatial Structure in Liquid Water. *Science* **1994**, *265*, 1219–1221.
- (77) Snyman, J. *Practical Mathematical Optimization An Introduction to Basic Optimization Theory and Classical and New Gradient-Based Algorithms*; Springer: New York, 2005; pp 57–93.
- (78) Pastor, R. W.; Brooks, B. R.; Szabo, A. An Analysis of the Accuracy of Langevin and Molecular Dynamics Algorithms. *Mol. Phys.* **1988**, *65*, 1409–1419.
- (79) Uberuaga, B. P.; Anghel, M.; Voter, A. F. Synchronization of Trajectories in Canonical Molecular-Dynamics Simulations: Observation, Explanation, and Exploitation. *J. Chem. Phys.* **2004**, *120*, 6363.
- (80) Berendsen, H. J. C.; Postma, J. P. M.; van Gunsteren, W. F.; DiNola, A.; Haak, J. R. Molecular Dynamics with Coupling to an External Bath. *J. Chem. Phys.* **1984**, *81*, 3684.
- (81) Oppenheim, A. V., W., S. R. *Discrete-Time Signal Processing*, 2nd ed.; Prentice-Hall: Upper Saddle River, NJ, 1999; pp 172–176.
- (82) Johnson, J. B. Thermal Agitation of Electricity in Conductors. *Phys. Rev.* **1828**, *32*, 97–109.
- (83) Nyquist, H. Thermal Agitation of Electric Charge in Conductors. *Phys. Rev.* **1928**, *32*, 110–113.
- (84) Bulashenko, O. M.; Kochelap, V. A. Johnson–Nyquist Noise for a 2D Electron Gas in a Narrow Channel. *J. Phys.: Condens. Matter* **1993**, *5*, L469–L474.
- (85) Weaver, J. C.; Astumian, R. D. The Response of Living Cells to very Weak Electric Fields: the Thermal Noise Limit. *Science* **1990**, *247*, 459–462.
- (86) Colombari, P. *Proton Conductors; Solids, Membranes and Gels—Materials and Devices*; Cambridge University Press: Cambridge, UK, 1992; pp 38–60.
- (87) Sellner, B.; Valiev, M.; Kathmann, S. M. Charge and Electric Field Fluctuations in Aqueous NaCl Electrolytes. *J. Phys. Chem. B* **2013**, *117*, 10869–10882.
- (88) Laio, A.; Parrinello, M. Escaping Free-Energy Minima. *Proc. Natl. Acad. Sci. U.S.A.* **2002**, *99*, 12562–12566.